ACS APPLIED MATERIALS & INTERFACES

Research Article

www.acsami.org

Uniform Carbon Layer Coated Mn_3O_4 Nanorod Anodes with Improved Reversible Capacity and Cyclic Stability for Lithium Ion Batteries

Changbin Wang, Longwei Yin,* Dong Xiang, and Yongxin Qi

Key Laboratory for Liquid−Solid Structural Evolution and Processing of Materials, Ministry of Education, School of Materials Science and Engineering, Shandong University, Jinan 250061, P. R. China

Supporting Information

ABSTRACT: A facile one-step solvothermal reaction route to large-scale synthesis of carbon homogeneously wrapped manganese oxide (Mn_3O_4@C) nanocomposites for anode materials of lithium ion batteries was developed using manganese acetate monohydrate and polyvinylpyrrolidone as precursors and reactants. The synthesized Mn_3O_4@C nanocomposites were characterized by X-ray diffraction, field-emission scanning electron microscopy, high resolution transmission electron microscopy, X-ray photoelectron spectroscopy, and Raman spectroscopy. The synthesized tetragonal structured Mn_3O_4 (space group *I*41/*amd*) samples display nanorodlike morphology, with a width of about 200−300 nm and a thickness of about 15−20 nm. It is shown that the carbon layers with a thickness of 5 nm are homogeneously coated on the Mn_3O_4 nanorods. It is indicated from lithium storage capacity estimation that the Mn_3O_4@C samples display enhanced capacity retention on charge/discharge cycling. Even after 50 cycles, the products remains stable capacity of 473 mA h g^{-1}, which is as much 3.05 times as that of pure Mn_3O_4 samples. Because of the low-cost, nonpollution, and stable capacity, the carbon homogeneously coated Mn_3O_4@C nanocomposites are promising anode material for lithium ion batteries.

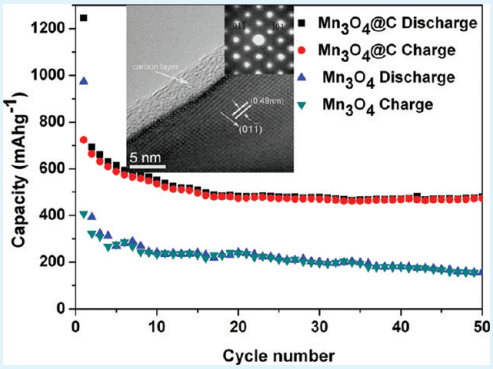

KEYWORDS: *manganese oxide, carbon, composite, microstructure, lithium ion battery*

1. INTRODUCTION

Lithium ion battery is one of the most suitable candidates to satisfy the energy requirements because of its high energy density, high voltage, and light weight. Electrode material is a determining factor for the battery performance. In commercial lithium ion batteries, the carbonaceous materials are generally used as anode materials.[1] However, the theoretical capacity of graphite is only 372 mA h g^{-1}. In recent years, metal oxide nanomaterials[2,3] (such as CoO_x,[4] FeO_x,[5,6] VO_x,[7] SnO_2,[8,9] MnO_x,[10,11] etc.) used as anode materials for lithium ion batteries have attracted much attention for their higher theoretic specific capacity than graphite. For the nanostructured oxide materials used as electrode applications, one problem is that the high surface area inevitably raises the risk of secondary reactions involving electrolyte decomposition between electrode and electrolyte,[12] which causes a high level of irreversibility (i.e., low columbic efficiency) and poor life cycle, and the formation of thick solid electrolyte interphase (SEI) films on the electrode surface, which consumes much of the Li supplied by the cathodes. Another major drawback affecting the practical applications of nanostructured oxides is their poor cycling performance caused by volume expansion during the charge−discharge process. To tackle this problem, researchers have taken various strategies.[13−16]

The surface modification[17] of electrode materials, including mild oxidation, deposition of metals and metal oxides, coating with polymers and some kinds of carbons, is proved to be an effective way to improve the cycling performance of electrode materials.[18] A general strategy of nanocoating the active materials with carbon is proved to be very practical with promising lithium ion battery performance.[8] It acts as a buffer layer that cushions the stress induced by volume expansion/contraction. Its elastic nature renders it very effective in accommodating the volume strain,[19] leading to a better capacity retention. At the same time, it also increases the electronic conductivity of the nanocomposite electrode. It has been proven that the coated carbon layer would protect the metal oxides from chemical corrosion and volumetric expansion.[20,21] It is reported that the carbon-contained oxide samples can be obtained as the oxide powder[22] were milled with sugar (as carbon source) and further sintered under an inert atmosphere, and the cyclic performance for lithium ion batteries were significantly improved. Using polyvinylpyrrolidone (PVP) as capping agent, ethylene glycol (EG) as reducing agent and ammonium heptamolybdate tetrahydrate (AHM) as molybde-

Received: December 16, 2011
Accepted: March 6, 2012
Published: March 6, 2012

dx.doi.org/10.1021/am2017909 | ACS Appl. Mater. Interfaces 2012, 4, 1636−1642

num source,[23] Wang et al. synthesized carbon-coated MoO_2 nanospheres for lithium ion batteries, showing high reversible capacity.

Among variety of metal oxides, manganese oxide[13,15,16] has aroused much interest as the anode materials in lithium ion batterey applications for its low cost, abundant resources, and nonpollution. Compared with other types of manganese oxides, there is few report about the study on Mn_3O_4 as anode materials for lithium ion battery applications,[14] maybe because of its extremely low electrical conductivity ($\sim 1 \times 10^{-7}$ to 1×10^{-8} S/cm). Pasero[10] found that the incorporation of Co into Mn_3O_4 could lead to a dramatic increase in electrochemical performance. However, the capacity is still only 400 mA h g^{-1} at a current density of 33−50 mAg^{-1}. Fan et al recently reported Mn_3O_4 nanofibers by electrospinning a solution of polymethylmethacrylate and manganese acetate,[24] and obtained a low electrochemical capacity from the Mn_3O_4 nanofiber anode. Recently, Dai[25] reported Mn_3O_4−graphene composite as capacity anode material for lithium ion batteries, whereas the synthesis process is complex and the graphene is costly.

Herein, we report the synthesis of carbon wrapped manganese oxide (Mn_3O_4@C) nanocomposites using hydrothermal method. Cyclic voltammetry (CV) and galvanostatic charge/discharge experiments were carried out to evaluate the electrochemical behaviors of the Mn_3O_4@C nanocomposites. The results showed that Mn_3O_4@C composites were suitable for the anode of lithium ion batteries, with a high specific capacity of 473 mA h g^{-1} achieved in Mn_3O_4@C electrode even after 50 cycles, almost as much 3.05 times as that pure Mn_3O_4 electrode. The Mn_3O_4 nanorods wrapped in carbon display a high and stable charge/discharge capacity, and can find potential applications as anode material for lithium ion batteries.

2. EXPERIMENTAL SECTION

2.1. Materials Synthesis. The Mn_3O_4@C nanocomposites were synthesized by hydrothermal reaction of a mixture solution of 20 mL of manganese acetate monohydrate (MAM) solution (6 mM), 3 mL of ethylene glycol (EG) (The EG in this reaction may act as the nuclei in the initial stage, guiding the growth of manganese oxide,[26] not as reducing agent.), 15 mL of polyvinylpyrrolidone (PVP) (MW: 58 000) solution (0.1 g mL^{-1}) and 25 mL of deionized (DI) water in a 100 mL Teflon-lined autoclave at 180 °C for 48 h. The brownish red products were collected by 3 centrifuge disperse-rinse cycles with DI water, and dried at 60 °C under vacuum. The as-synthesized samples were further annealed at 700 °C for 4 h in a N_2 flow to obtain the final brownish black products of Mn_3O_4@C nanocomposites. The synthesis of pure Mn_3O_4 was the same as above-mentioned but without PVP.

2.2. Structural Characterization. The powder X-ray diffraction (XRD) patterns of the products were determined by Rigaku D/Max-KA diffractometer equipped with Cu Ka radiation. The morphology and chemical components of the products were analyzed using SU-70 field emission scanning electron microscopy (FE-SEM), respectively. The morphology and microstructure of the synthesized products were analyzed using high-resolution transmission electron microscopy (HR-TEM) of Tecnai 20U-Twin at an acceleration voltage of 200 kV. Raman spectrum was recorded using a Horiba Jobin-Yvon micro Raman spectrometer, equipped with a microscope and a 633 nm laser as the excitation source. X-ray photoelectron spectroscopy (XPS) characterization was carried out in an ESCALAB 250 instrument with 150W Al Ka probe beam. Survey and multiregion spectra were recorded at Mn 2p, C1s, and O1s photoelectron peaks. Thermogravimetric analysis (TGA) was carried out under a flow of air with a temperature ramp of 10 °C min^{-1} from 40 to 800 °C using thermogravimetric analyzer (TG-209C).

2.3. Electrochemical Determination. The galvanostatic charging/discharging tests were conducted using standard 2025 type coin cells with copper foil as the current collectors, lithium foil as reference electrodes and 1.0 M $LiPF_6$ in mixed ethylene carbonate (EC) and diethyl carbonate (DEC) (EC:DEC, 1:1 by volume) as the electrolyte. A cutoff voltage window of 0.01−3.0 V is used. The working electrode is composed of Mn_3O_4@C nanoparticles, carbon black (super-P-Li), and polyvinylidene difluoride (PVDF) in a weight ratio of 70:15:15. The mass of active materials is around 1−2 mg, depending on the thickness of film formed on Cu current collector. The 2025 coin-type cells were galvanostatically cycled on a LAND CT2001A instrument (Wuhan, China) at room temperature. Cyclic voltammetry (CV) study was conducted using an electrochemical workstation (PARSTAT 2273) between 0.01 − 2.0 V at a scan rate of 0.1 mV s^{-1}.

3. RESULTS AND DISCUSSION

3.1. XRD Characterization of Mn_3O_4@C Samples. Figure 1 shows a typical XRD spectrum of the synthesized

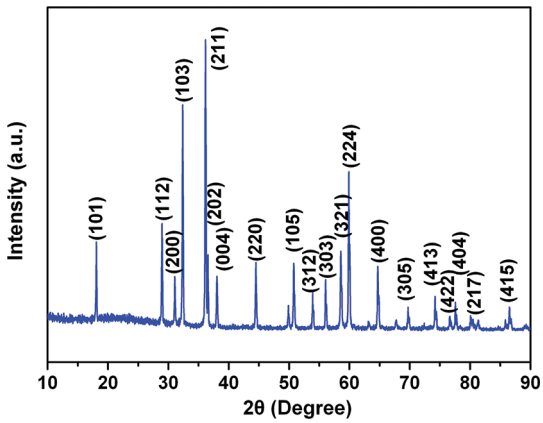

Figure 1. XRD pattern of the Mn_3O_4@C nanocomposites.

products. It is indicated that the synthesized products are composed of only hausmannite Mn_3O_4 with tetragonal structure (space group $I41/amd$) with lattice constants of a = 5.76 Å, c = 9.47 Å, corresponding to that of JCPDS 24−0734. The diffraction peaks at 18.0°, 28.9, 31.0, 32.3, 36.1, 38.0, and 44.4° positions can be well-assigned to (101), (112), (200), (103), (211), (004), and (220) planes of the hausmannite Mn_3O_4 with tetragonal structure. The carbon was not detected, mybe due to the amorphous state for the carbon, and no other impurity phases were observed in the synthesized products.

3.2. SEM and TEM Characterization of Mn_3O_4@C Samples. The microstructures of the Mn_3O_4@C samples are observed by field emission scanning electron microscopy (FE-SEM), as shown in Figure 2. From overall SEM image in Figure 2a, it is shown that large scale of synthesized products in the form of thin film can be obtained. From side view SEM image of the samples shown in Figure 2b, it clearly indicates that the Mn_3O_4 nanocrystals arrange as the parallel arrays in the thin film. The thickness of the Mn_3O_4 parallel arrays is about 4−5 μm. The top view SEM image shown in Figure 2c suggests that the synthesized Mn_3O_4 nanocrystals display nanorod like morphology, the width of the Mn_3O_4 nanorods is about 200−300 nm, and the thickness of the Mn_3O_4 nanorods is about 15−20 nm. Figure 2d demonstrates a typical magnified SEM image of the Mn_3O_4 nanorods, showing the polygonous nature of the nanorods. Figure 3 depicts a X-ray energy-dispersive spectroscopy (EDS) spectrum, suggesting the synthesized products are composed of Mn, O, and C elements.

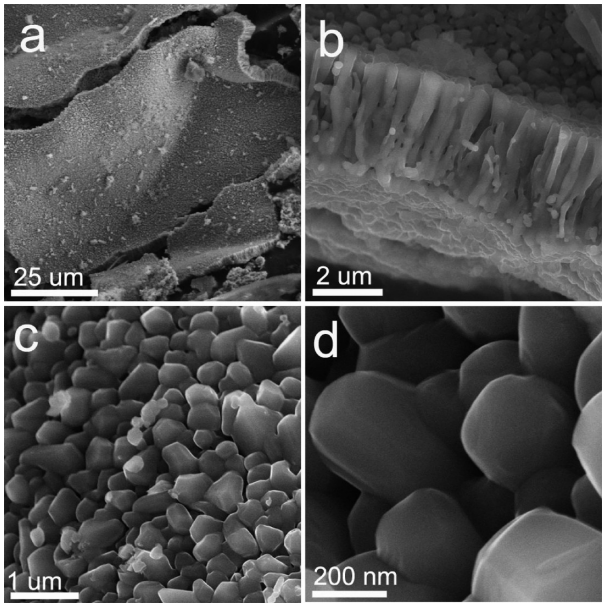

Figure 2. FE-SEM images of Mn_3O_4@C nanocomposites. (a) Low magnification, (b) side view, (c, d) high magnification.

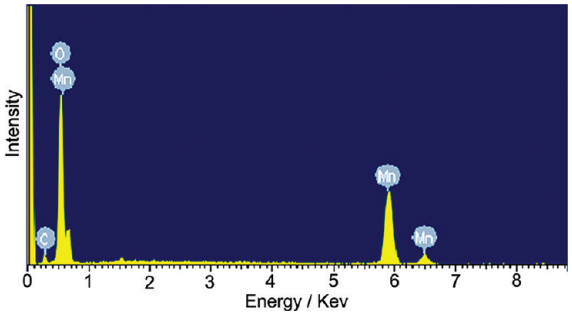

Figure 3. EDS spectrum from the synthesized carbon wrapped Mn_3O_4 nanorods.

Transmission electron microscopy was used to further reveal the detailed microstructures of the carbon wrapped Mn_3O_4 nanorod samples. Figure 4a depicts a low-magnification TEM image of the Mn_3O_4@C sample. It is clearly illustrated that a thin layer is homogeneously covered on the surfaces of the Mn_3O_4 nanorods. Figure 4b gives a typical high resolution transmission electronmicropy (HRTEM) lattice image from the carbon wrapped Mn_3O_4 nanorods. The thickness of the carbon

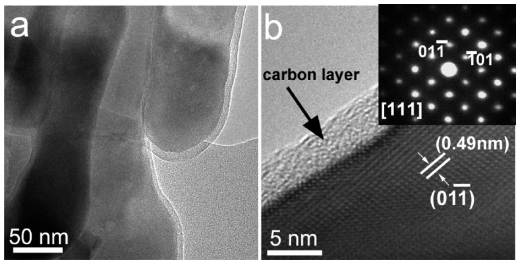

Figure 4. TEM images of Mn_3O_4@C samples. (a) Low-magnification TEM image. (b) High-resolution transmission electron microscopy (HRTEM) lattice image obtained along [111] zone axis, the marked 0.49 nm spacing in Figure 3b corresponds well with *d*-spacing of (011) planes of tetragonal Mn_3O_4, the inset right upper side is the corresponding electron diffraction pattern along the [111] zone axis.

layer is about 5 nm. The inset right upper side is the corresponding selected electron diffraction pattern along the [111] zone axis of the Mn_3O_4, indicating the single crystalline nature of the tetragonal Mn_3O_4. The marked *d*-spacing of 0.49 nm in Figure 4b corresponds well with that of (011) planes of tetragonal Mn_3O_4 (space group: $I41/amd$) with lattice constants of a = 5.76 Å, c = 9.47 Å. It directly indicates from the HRTEM lattice image that the Mn_3O_4 nanorods are single crystalline.

3.3. TGA Characterization of Mn_3O_4@C Samples. To accurately determine the content of carbon in Mn_3O_4@C composites, thermogravimetry analyses (TGA) was carried out under air from 40 to 800 °C with a temperature ramp of 10 °C min^{-1} (Figure 5). From room temperature to 250 °C, there was

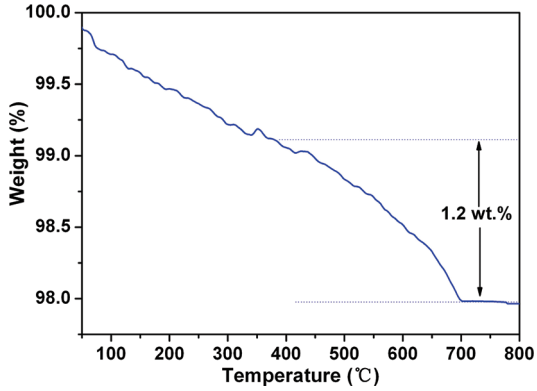

Figure 5. TGA curves of the Mn_3O_4@C composites under air at a rate of 10 °C min^{-1} from 40 to 800 °C.

little change because of the loss of free water and physically adsorbed water, whereas from 250 to 350 °C, the weight loss was ascribed to the simultaneous loss of coordinated water.[27] When the temperature increased to 350 °C, the carbon started to decompose, and completely disappeared at about 700 °C. Thus, the mass ratio of carbon was about 1.2%.

3.4. XPS Spectra of Mn_3O_4@C Sample. To investigate the chemical composition and chemical bonding state of the synthesized carbon wrapped Mn_3O_4 nanorods, we further characterized the sample by X-ray photoelectron spectroscopy (XPS). Figure 6a shows a typical overal XPS spectrum of the Mn_3O_4@C nanocomposites, suggesting that the nanocomposistes are composed of Mn, O, and C elements. Figure 6b depicts the XPS spectrum of Mn 2p, where two peaks located at 641.9 and 653.5 eV can be attributed to Mn $2p_{3/2}$ and Mn $2p_{1/2}$ levels, respectively. The bonding energies at the Mn $2p_{3/2}$ and Mn $2p_{1/2}$ peaks agree well with that of reported for Mn_3O_4,[28] indicating oxidation state for Mn. Figure 6c shows the deconvoluted O 1s spectrum, where three peak located at 529.5, 530.8, and 532.2 eV can be observed. This spectrum is in good agreement with reported values of 529.3−530.3 eV for oxide, 530.5−531.5 eV for hydroxide, and 531.8−532.8 eV for water.[29] The spectrum of C 1s can be observed from Figure 6d. Three sharp peaks at binding energies of 283.7, 284.9, and 285.9 eV, correspond to highly oriented pyrolytic graphite, amorphous carbon and carbon−hydrogen functional group, respectively.[30] Corresponding to carbon layer on surface of Mn_3O_4 nanorod in HRTEM image in Figure 4b, the coated carbon is in the form of amorphous phase.

3.5. Raman Characterization of Mn_3O_4@C Sample. The nature and type of carbon is further characterized by Raman

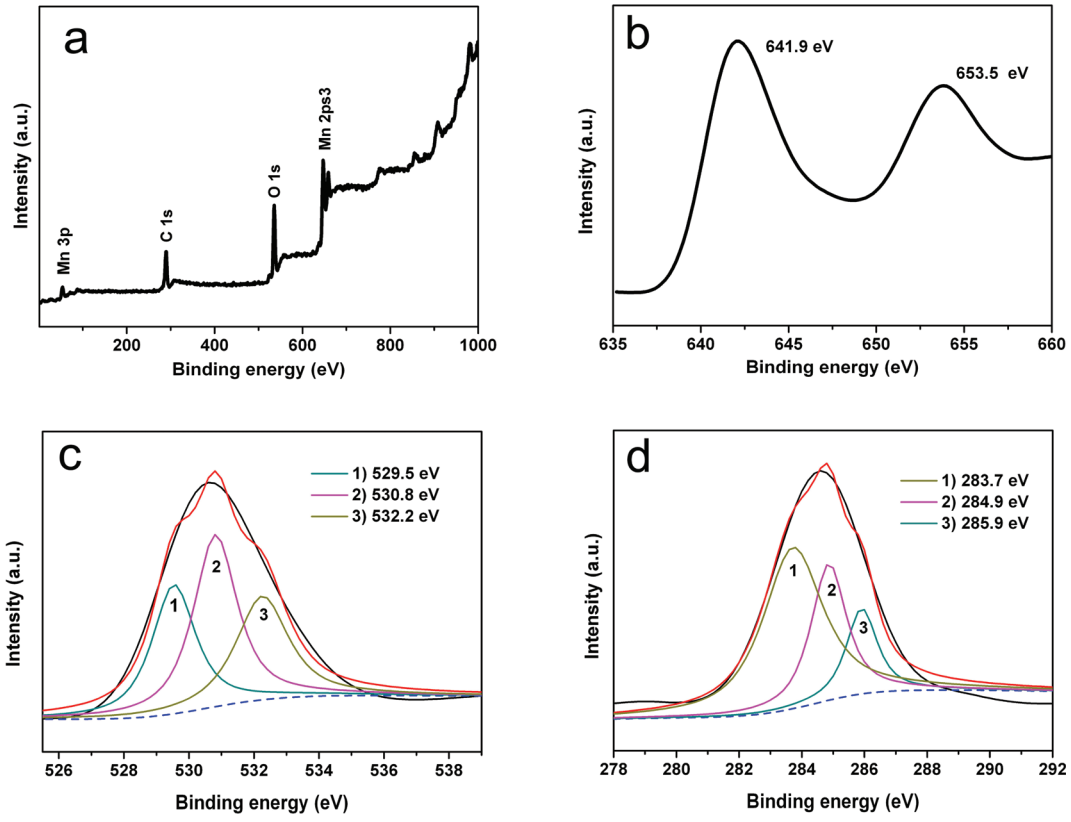

Figure 6. XPS spectra of Mn_3O_4@C after annealing at 700 °C. (a) Survey scan, (b) Mn 2p, (c) O 1s, and (d) C 1s spectra.

measurements. The two major Raman bands located at 1331 and 1603 cm^{-1} (Figure 7). The band at 1331 cm^{-1} corresponds

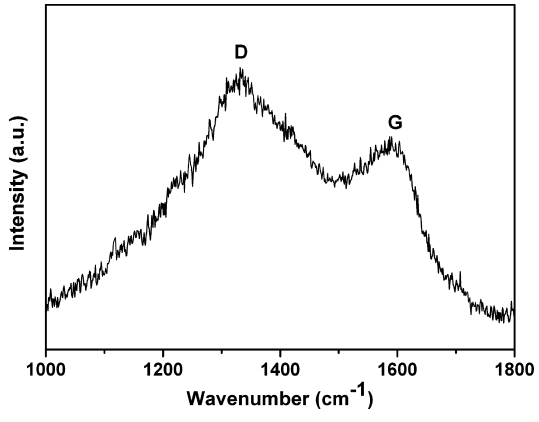

Figure 7. Raman spectrum of the product after annealing at 700 °C.

to the D peak arising from the breathing motion of sp^2 rings, and the band at 1603 cm^{-1} is in good agreement with the G band. The ratio between the D and G bands is found to be correlated to the nature of carbon.[20] The measured intensity I_D/I_G ratio is about 1.35, suggesting that the carbon exists in a disordered graphitic form (amorphous), which is in conformity with the XPS spectra of carbon and the HR-TEM results.

3.6. Electrochemical Characterization of Mn_3O_4@C Sample. The carbon-wrapped Mn_3O_4 nanostructures make them promising for applications in energy storage. The electrochemical performance of the Mn_3O_4@C nanocomposite electrode as anode material for lithium-ion batteries was investigated. Figure 8a shows the voltage profiles of the 1st, 5th,

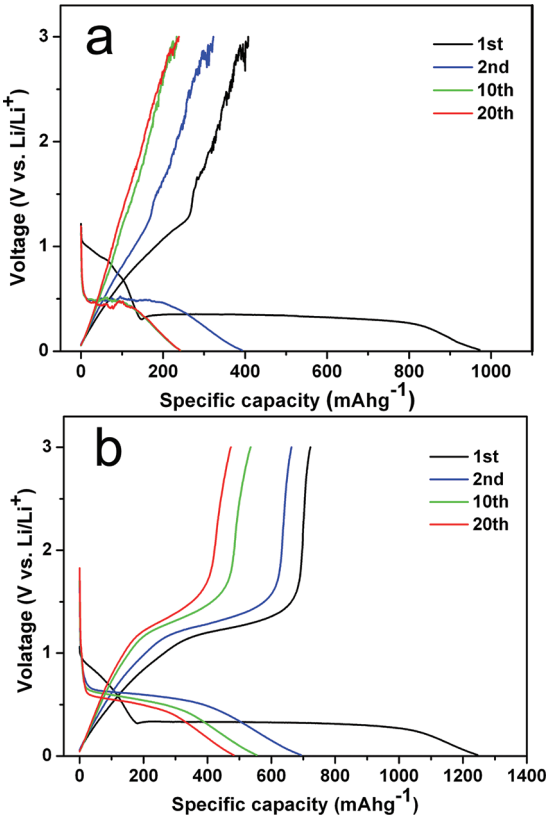

Figure 8. (a) 1st, 2nd, 10th, 20th voltage of the Mn_3O_4 electrode between 0.01 and 3 V at the current of 40 mA g^{-1}. (b) 1st, 2nd, 10th, 20th voltage of the Mn_3O_4@C electrode between 0.01 and 3 V at the current of 40 mA g^{-1}.

dx.doi.org/10.1021/am2017909 | ACS Appl. Mater. Interfaces 2012, 4, 1636–1642

10th, and 20th cycles for the pure Mn_3O_4 nanorod electrode cycled between 0.01 and 3 V at a current density of 40 mA g^{-1}. The first discharge and charge capacities are 974 and 407 mA h g^{-1}, respectively, and the Coulombic efficiency is 41.8%, whereas for the Mn_3O_4@C nanocomposites (Figure 8b), the first discharge and charge capacities are 1246 and 723 mA h g^{-1}, respectively, and the Coulombic efficiency is 58.0%. From the second cycle, the carbon-wrapped Mn_3O_4@C nanocomposite electrode displays much better electrochemical lithium storage performance than pure Mn_3O_4 electrode. After ten discharge/charge cycles, it exhibits a high reversible capacity of 557 mA h g^{-1} for the Mn_3O_4@C nanocomposite electrode, the Coulombic efficiency rapidly rises from 58.0% in the first cycle to 96.3% in the tenth cycle and then remains above 98% in the following cycles. In contrast, after 10 discharge/charge cycles, the pure Mn_3O_4 electrode exhibits a reversible capacity of 245 mA h g^{-1}, the Coulombic efficiency rapidly rises from 41.8% in the first cycle to 96.3% in the tenth cycle and then remains about 95% in the following cycles. It is obviously indicated that the Mn_3O_4@C nanocomposite electrode displays a much higher reversible capacity than the pure Mn_3O_4 electrode. More importantly, from the trend of diagram, the voltage curve of the absolute Mn_3O_4 is rough, while the voltage curve of Mn_3O_4@C is smooth, indicating more stability of the electrochemistry of the Mn_3O_4@C nanocomposites.

To better illustrate the redox reactions, we measured cyclic voltammetric (CV) curves for the first five cycles of Mn_3O_4@C and pure Mn_3O_4 electrodes, as shown in Figure 9. The first

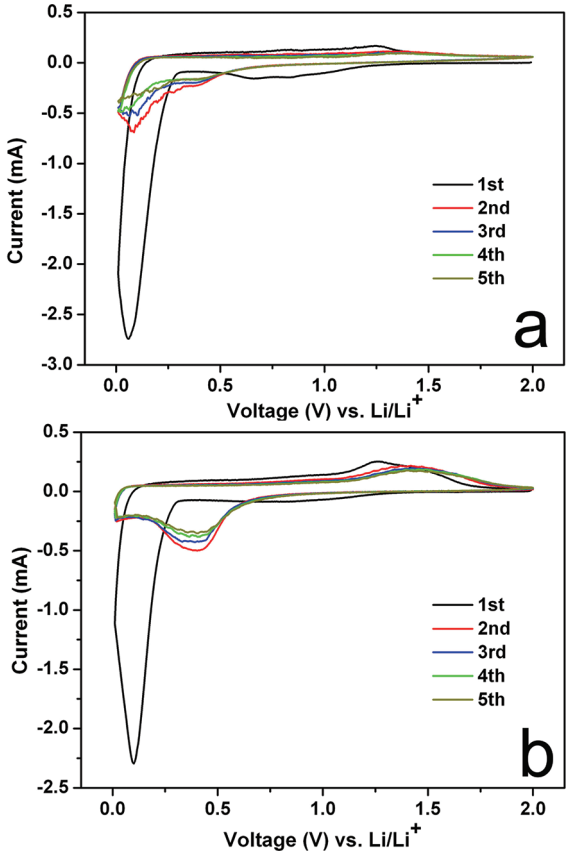

Figure 9. Cyclic voltammetric (CV) curves of the first five cycles for the Mn_3O_4@C and the pure Mn_3O_4 electrodes at a scan rate of 0.1 mV s^{-1} between 0.01 and 2.0 V.

lithium insertion/extreaction process for both the Mn_3O_4@C and the pure Mn_3O_4 electrodes displayed quite different reaction profiles in the cathodic sweep and similar oxidation peak position in the anodic sweep compared with the following ones. Respectively, at around ~0.1 V vs Li/Li^+, both the electrochemical reactions were highly irreversible. The irreversible capacity corresponding to the voltage range of 1.1−0.1 V of the first electrode materials discharge curve was attributed to the formation of a solid electrolyte interphase (SEI) layer and decomposition of electrolyte solvent between the electrode and electrolyte. Besides these, this irreversible capacity was also attributed to the irreversible reaction between Li^+ and carbon of the Mn_3O_4@C electrode.[25] Compared with Figure 8, the formation of Mn and Li_2O at about 0.3 V can be described by the electrochemical conversion reaction.[14,25]

$$Mn_3O_4 + 8Li^+ + 8e^- \rightarrow 4Li_2O + 3Mn$$

The slope at the voltage of 1.1−0.3 V (also can be seen from Figure 8) mainly owed to reduction from Mn(III) to Mn(II),[10,25] whereas the discharge capacity in the rang of 0.3−0.1 V indicated the reduction from Mn(II) to Mn(0).[31] The charge curve (the anode sweep) showed a sloping voltage at about 1.3 V as a result of the reverse reaction between Li^+ and the electrodes.[25] From the second cycles, both the pure Mn_3O_4 and Mn_3O_4@C exhibited similar trend. The pure Mn_3O_4 reduction peak appeared at about 0.1 V while the Mn_3O_4@C shifted to 0.5 V indicating an irreversible phase transformation due to the formation of Li_2O and metallic manganese.[32] Both the oxidation peaks appeared at 1.4 V for the Mn_3O_4@C and Mn_3O_4 electrodes. Compared with the pure Mn_3O_4, the carbon coated Mn_3O_4 electrode displayed better reversibility, indicating better structural stability.

Figure 10 shows the cyclic performance of the pure Mn_3O_4 and Mn_3O_4@C nanocomposite electrodes. It can be found that

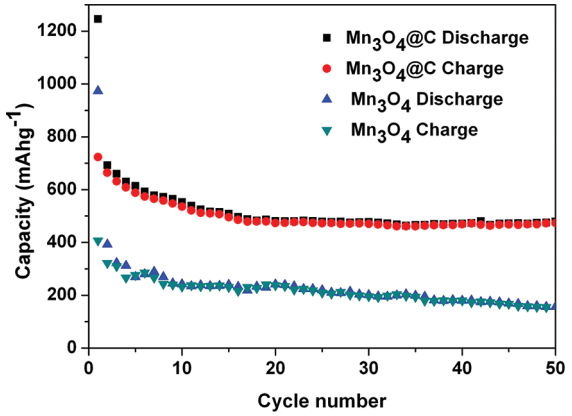

Figure 10. Capacity vs cycle number curves of the Mn_3O_4@C nanocomposites electrode (upper curve) and the pure Mn_3O_4 electrode (lower curve).

the Mn_3O_4@C nanocomposite electrode exhibits much better cycling stability than that of the pure Mn_3O_4 electrode. After the 10 cycles, the discharge capacity pure Mn_3O_4 nanoparticles are only 235 mA h g^{-1},whereas the Mn_3O_4@C nanocomposites are above 550 mA g h^{-1}, even after 50 cycles the Mn_3O_4@C can still remain 473 mA h g^{-1}, corresponding to 38.0% capacity retention. However, for the Mn_3O_4 electrode, a discharge capacity of 155 mA h g^{-1} can be obtained at the 50th cycle, corresponding to 15.9% capacity retention. After the 15th cycle,

dx.doi.org/10.1021/am2017909 | ACS Appl. Mater. Interfaces 2012, 4, 1636−1642

the discharge of Mn_3O_4@C remains stable, and the Coulombic efficiency can keep between 98.5 and 99.6, displaying good reversibility.

To further understand the effect of the uniform carbon layer on the surface of manganese oxide electrode, we measured the FE-SEM after the half sells cycled 10 times (see the Supporting Information). The enhanced electrochemical performance of Mn_3O_4@C nanocomposites can be attributed to the improved kinetics for lithium intercalation/deintercalation.[23] The uniform length and width of the Mn_3O_4 nanorods favored the diffusion of Li^+ ions between the electrodes. The nanorods of Mn_3O_4 with large surface area offered more active sites for the Li^+ ions insertion/extraction.[32] The amorphous carbon layer on the surface of Mn_3O_4 nanorods acts as block to prevent the aggregation of manganese nanoparticles.[20,23] It presented that even after 10 cycles the carbon coated Mn_3O_4 nanorods electrode (see Figure S1c in the Supporting Information) maintained good structure stability, however, the bare Mn_3O_4 nanorods (see Figure S1d in the Supporting Information) were crushed after the lithium insertion and extraction. Further more, the carbon layer distinctly enhanced cycling stability through protecting the metal oxides from chemical corrosion[20,33] and buffering the stress caused by volume change.[34] The elastic nature of carbon renders it very effective in accommodating the volume strain,[8] leading to a better capacity retention. At the same time, the carbon layer also increases the electronic conductivity of both the nanocomposite electrode[35] and the SEI layer and restrain the interaction between the anode material and electrolyte.[36] Last but not least, the metal oxide electrode cycling performance is influenced by the SEI layer, whereas the carbon layer could make SEI films more stable on the nanocomposite surface, which is under much smaller volume changes,[21] and the SEI film formed on the carbon layer could be retained well in each cycle progress to consume the stored Li capacity.[37,38]

4. CONCLUSIONS

In summary, we have demonstrated a one-pot hydrothermal route to synthesize carbon-coated uniform Mn_3O_4 nanorod nanocomposites. The synthesized Mn_3O_4 samples with tetragonal structure (space group: *I*41/*amd*) display nanorod-like morphology, with a width of about 200−300 nm and a thickness of about 15−20 nm. The carbon layers with a thickness of 5 nm are homogeneously coated on the Mn_3O_4 nanorods. The carbon layer homogeneously coated Mn_3O_4 nanorod samples display enhanced lithium storage than that of pure Mn_3O_4. Cyclic voltammetry (CV) and galvanostatic charge/discharge experiments were carried out to evaluate the electrochemical behaviors of the Mn_3O_4@C nanocomposites. The results showed that Mn_3O_4@C composites were suitable for the anode of lithium ion batteries, with a high specific capacity of 473 mA h g^{-1} achieved in Mn_3O_4@C electrode even after 50 cycles, almost 3.05 times as much as that of pure Mn_3O_4 electrode. The Mn_3O_4 nanorods wrapped in carbon display a high and stable charge/discharge capacity, and can find potential applications as anode material for lithium ion batteries.

■ ASSOCIATED CONTENT

Supporting Information

This material is available free of charge via the Internet at http://pubs.acs.org.

■ AUTHOR INFORMATION

Corresponding Author

*Tel.: + 86 531 88396970. Fax: + 86 531 88396970. E-mail: yinlw@sdu.edu.cn.

Notes

The authors declare no competing financial interest.

■ ACKNOWLEDGMENTS

We acknowledge support from the National Natural Science Funds for Distinguished Young Scholars (51025211), National Nature Science Foundation of China (50972079), the Shandong Natural Science Fund for Distinguished Young Scholars (JQ200915), the Foundation of Outstanding Young Scientists in Shandong Province (2006BS04030), the Tai Shan Scholar Foundation of Shandong Province.

■ REFERENCES

(1) Zheng, H. H.; Jiang, K.; Abe, T.; Ogumi, Z. *Carbon* **2006**, *44*, 203.
(2) Poizot, P.; Laruelle, S.; Grugeon, S.; Dupont, L.; Tarascon, J. M. *Nature* **2000**, *407*, 496.
(3) Nam, K. T.; Kim, D. W.; Yoo, P. J.; Chiang, C. Y.; Meethong, N.; Hammond, P. T.; Chiang, Y. M.; Belcher, A. M. *Science* **2006**, *312*, 885.
(4) Kang, Y. M.; Song, M. S.; Kim, J. H.; Kim, H. S.; Park, M. S.; Lee, J. Y.; Liu, H. K.; Dou, S. X. *Electrochim. Acta* **2005**, *50*, 3667.
(5) Chowdari, B. V. R.; Reddy, M. V.; Yu, T.; Sow, C. H.; Shen, Z. X.; Lim, C. T.; Rao, G. V. S. *Adv. Funct. Mater.* **2007**, *17*, 2792.
(6) Chen, J. S.; Zhang, Y. M.; Lou, X. W. *ACS Appl. Mater. Interfaces* **2011**, *3*, 3276.
(7) Xie, Y.; Zhang, S. D.; Li, Y. M.; Wu, C. Z.; Zheng, F. *J. Phys. Chem. C* **2009**, *113*, 15058.
(8) Derrien, G.; Hassoun, J.; Panero, S.; Scrosati, B. *Adv. Mater.* **2007**, *19*, 2336.
(9) Liu, W. F.; Huang, X. J.; Wang, Z. X.; Li, H.; Chen, L. Q. *J. Electrochem. Soc.* **1998**, *145*, 59.
(10) Pasero, D.; Reeves, N.; West, A. R. *J. Power Sources* **2005**, *141*, 156.
(11) Ji, L. W.; Zhang, X. W. *Electrochem. Commun.* **2009**, *11*, 795.
(12) Bruce, P. G.; Scrosati, B.; Tarascon, J. M. *Angew. Chem., Int. Ed.* **2008**, *47*, 2930.
(13) Ammundsen, B.; Paulsen, J. *Adv. Mater.* **2001**, *13*, 943.
(14) Thackery, M. M.; David, W. I. F.; Bruce, P. G.; Goodenough, J. B. *Mater. Res. Bull.* **1983**, *18*, 461.
(15) Ajayan, P. M.; Reddy, A. L. M.; Shaijumon, M. M.; Gowda, S. R. *Nano Lett.* **2009**, *9*, 1002.
(16) Feng, Q.; Kanoh, H.; Ooi, K. *J. Mater. Chem.* **1999**, *9*, 319.
(17) Zhi, C. Y.; Bando, Y.; Tang, C. C.; Golberg, D. *J. Phys. Chem. B* **2006**, *110*, 8548.
(18) Holze, R.; Fu, L. J.; Liu, H.; Li, C.; Wu, Y. P.; Rahm, E.; Wu, H. Q. *Solid State Sci.* **2006**, *8*, 113.
(19) Mominuzzaman, S. M.; Krishna, K. M.; Soga, T.; Jimbo, T.; Umeno, M. *Carbon* **2000**, *38*, 127.
(20) Hwang, S. J.; Han, A. R.; Kim, T. W.; Park, D. H.; Choy, J. H. *J. .Phys. Chem. C* **2007**, *111*, 11347.
(21) Zhang, W. M.; Wu, X. L.; Hu, J. S.; Guo, Y. G.; Wan, L. J. *Adv. Funct. Mater.* **2008**, *18*, 3941.
(22) Li, H.; Zhong, K. F.; Xia, X.; Zhang, B.; Wang, Z. X.; Chen, L. Q. *J. Power Sources* **2010**, *195*, 3300.
(23) Wang, Z. Y.; Chen, J. S.; Zhu, T.; Madhavi, S.; Lou, X. W. *Chem. Commun.* **2010**, *46*, 6906.
(24) Fan, Q.; Whittingham, M. S. *Electrochem. Solid-State lett.* **2007**, *10*, A48.
(25) Wang, H. L.; Cui, L. F.; Yang, Y. A.; Casalongue, H. S.; Robinson, J. T.; Liang, Y. Y.; Cui, Y.; Dai, H. J. *J. Am. Chem. Soc.* **2010**, *132*, 13978.

(26) Xiao, W.; Chen, J. S.; Lu, Q.; Lou, X. W. *J. Phys. Chem. C* **2010**, *114*, 12048.
(27) Xiong, C. R.; Aliev, A. E.; Gnada, B.; Balkus, L. J. *ACS Nano* **2008**, *2*, 293.
(28) Di Castro, V.; Ciampi, S.; Sestili, L. *Surf. Rev. Lett.* **1998**, *5*, 393.
(29) Yan, D.; Yan, P. X.; Cheng, S.; Chen, J. T.; Zhuo, R. F.; Feng, J. J.; Zhang, G. A. *Cryst. Growth Des.* **2009**, *9*, 218.
(30) Ago, H.; Kugler, T.; Cacialli, F.; Salaneck, W. R.; Shaffer, M. S. P.; Windle, A. H.; Friend, R. H. *J. Phys. Chem. B* **1999**, *103*, 8116.
(31) Zhang, L. Z.; Xiao, L. F.; Yang, Y. Y.; Yin, J.; Li, Q. *J. Power Sources* **2009**, *194*, 1089.
(32) Wang, G. X.; Sun, B.; Chen, Z. X.; Kim, H. S.; Ahn, H. *J. Power Sources* **2011**, *196*, 3346.
(33) Lou, X. W.; Zhu, T.; Chen, J. S. *J. Phys. Chem. C* **2011**, *115*, 9814.
(34) Zhang, W. M.; Hu, J. S.; Guo, Y. G.; Zheng, S. F.; Zhong, L. S.; Song, W. G.; Wan, L. J. *Adv. Mater.* **2008**, *20*, 1160.
(35) Hu, Y. S.; Guo, Y. G.; Sigle, W.; Maier, J. *Adv. Mater.* **2007**, *19*, 2087.
(36) Shi, S. J.; Tu, J. P.; Zhang, Y. Q.; Guo, C. D.; Wang, X. L. *Electrochim. Acta* **2012**, *63*, 112.
(37) Li, H.; Hu, J.; Huang, X. J.; Chen, L. Q. *Solid State Ionics* **2006**, *177*, 2791.
(38) Zhou, Z.; Yuan, S. M.; Li, J. X.; Yang, L. T.; Su, L. W.; Liu, L. *ACS Appl. Mater. Interfaces* **2011**, *3*, 705.